Multivariate Phase Space Warping-Based Degradation Tracking and Remaining Useful Life Prediction of Rolling Bearings

Hengyu Liu, *Graduate Student Member, IEEE*, Rui Yuan, *Member, IEEE*, Yong Lv, Xingkai Yang, Hewenxuan Li, and Ersegun Deniz Gedikli

***Abstract*—Effective utilization of signals collected by distributed sensor networks is crucial for tracking degradation and forecasting the remaining useful life (RUL) of rolling bearings. The phase space warping (PSW) algorithm constructs the hierarchical dynamics to physically describe damage evolution. However, the PSW algorithm is unable to handle multivariate signals. To enable synchronous tracking of degradation in multivariate signals, the proposed solution is the multivariate phase space warping (MPSW) algorithm. First, the multivariate signals are embedded in the reconstructed phase space. Second, the local polynomial receives the current phase space trajectory (PST) to predict the reference PST, after which damage indicators are extracted by comparing the current PST with the reference PST. Third, robust principal component analysis with tensor smooth constraint was proposed on the DIs tensor to extract the main degradation pattern. Finally, the degradation is input to the exponential degradation model to predict the RUL. The run-to-failure experimental datasets for rolling bearings are applied to validate the effectiveness of the proposed MPSW. Experimental results demonstrate that the proposed MPSW effectively tracks the multivariate degradation, and accurately predicts the RUL with distributed sensor networks.**

***Index Terms*—Degradation tracking, multivariate signal processing, phase space warping (PSW), prognostics and health management, remaining useful life (RUL) prediction, rolling bearings.**

Manuscript received 4 December 2023; revised 30 December 2023; accepted 30 January 2024. Date of publication 14 February 2024; date of current version 4 September 2024. This work was supported in part by the National Natural Science Foundation of China under Grant 52305125 and Grant 51875416, in part by the Hubei Provincial Natural Science Foundation Youth Program, Innovation Group Program, and Innovation Development Joint Key Program under Grant 2023AFB028, Grant 2020CFA033, and Grant 2023AFD001, in part by Wuhan Key Research and Development Plan Artificial Intelligence Innovation Special Program under Grant 2023010402040005, and in part by the 14th Five Year Plan Hubei Provincial Advantaged Characteristic Disciplines (Groups) Project of Wuhan University of Science and Technology under Grant 2023B0301. Associate Editor: Y. Deng. *(Corresponding author: Rui Yuan.)*

Hengyu Liu, Rui Yuan, and Yong Lv are with the Key Laboratory of Metallurgical Equipment and Control Technology, Ministry of Education, Wuhan 430081, China, and also with the Hubei Key Laboratory of Mechanical Transmission and Manufacturing Engineering, Wuhan University of Science and Technology, Wuhan 430081, China (e-mail: liuhengyu@wust.edu.cn; yuanrui@wust.edu.cn; lvyong@wust.edu.cn).

Xingkai Yang is with the Mechanical Engineering Department, University of Alberta, Edmonton, AB T6G 1H9, Canada (e-mail: xingkai2@ualberta.ca).

Hewenxuan Li is with the Laboratory for Intelligent Systems and Controls, Cornell University, Ithaca, NY 14850 USA (e-mail: hewenxuan.li@cornell.edu).

Ersegun Deniz Gedikli is with the Department of Ocean and Resources Engineering, University of Hawaii at Manoa, Honolulu, HI 96822 USA (e-mail: egedikli@hawaii.edu).

Digital Object Identifier 10.1109/TR.2024.3361717

I. Introduction

THE prognostics and health management (PHM) of mechanical systems are vital for ensuring production efficiency and safety. Extensive research in PHM has led to the evolution of maintenance strategies for mechanical systems, shifting from traditional breakdown maintenance to predictive maintenance [1], [2]. Predictive maintenance relies on the condition monitoring of mechanical systems to predict future degradation trends and guide maintenance strategies [3]. Accelerometers are commonly installed on mechanical equipment to collect vibration signals, which are then analyzed to determine equipment health conditions [4]. Nevertheless, location of faults in complex mechanical systems is usually unknown, and incorrect places for sensor installation obscure the fault signatures. Therefore, distributed sensor networks are utilized to collect more comprehensive damage indicators (DIs) about health conditions [5]. To achieve predictive maintenance with multi-sensors, simultaneous extraction of the damage state from multivariate signals and predict the remaining useful life (RUL) are necessary.

The RUL accuracy is related to the accuracy of the DIs extracted from vibration signals of mechanical systems. In the study of degradation tracking, many researchers have proposed algorithms based on the time domain, frequency domain, and machine learning algorithms. Wang and Tsui [6] proposed a new health index based on the square envelope algorithm, which sensitively reflected early bearing defects. Ding et al. [7] proposed a new Bayesian approximation enhanced probabilistic meta-learning algorithm, which has a good calibration uncertainty effect in fault prediction. Zhang et al. [8] extracted main signal features to generate health indicators through hidden Markov model and principal component analysis. Most of the algorithms reviewed above were developed for single-sensor signal processing. The fault location cannot be known in advance of fault diagnosis. Improper sensor placement can decrease the efficacy of the degradation tracking as the vibration signal

collected from a wrongly placed sensor is insufficient to identify damage.

To make full use of the multiple sensors, many researchers have proposed damage extraction algorithms combined with information fusion. Liu et al. [9] proposed an approach with vector dynamic weighted fusion algorithm to evaluate the feature degradation sensitivity. The algorithm achieved feature fusion and improved the sensitivity of degradation tracking. Ayhan et al. [10] proposed a new bearing RUL adaptive prediction method, which reduces the risk of unstable results through parallel-running RUL predictors. Zhao et al. [11] proposed a model-assisted multi-source fusion hypergraph convolutional neural network to solve the problem of small-sample intelligent fault diagnosis of electrohydrostatic actuator. Xiong et al. [12] proposed an adaptive prediction framework for RUL prediction based on failure model recognition. The algorithm adaptively trained the model according to the recognition results and improved the RUL accuracy. Li et al. [13] referred to the Wiener process and particle filter to select the optimal sensor group from multiple sensors for information fusion. Compared with algorithms based on single sensor signals, the approaches introduced above have a stronger capability of the information fusion. However, most of them applied deep learning algorithms, which led to unclear physical properties of DIs extracted from signals.

For tracking mechanical system damage, several physical feature-based signal processing algorithms have been proposed. Lv et al. [14] proposed the multivariate empirical mode decomposition approach to diagnose rolling bearings, and successfully extract the fault characteristic frequencies from multivariate signals. Zhang et al. [15] proposed a multivariate dynamic mode decomposition algorithm to simultaneously extract fault features from multivariate signals, which improved the algorithm's robustness and effectiveness. Yuan et al. [16] improved the multivariate variational mode decomposition algorithm for application in condition monitoring of bolted connections. Cusumano and Chelidze [17] proposed the phase space warping (PSW) algorithm for general damage evolution and degradation tracking. Chelidze and Li [18] combined vibration signals with the physical evolution of machinery damage. The proposed PSW algorithm was successfully applied for tracking damage evolution of beam structures [19]. To predict the RUL, Qian et al. [20] employed a multidimensional autoregressive model in combination with a particle filter to enhance the PSW. Luo et al. [21] studied the optimal phase space (PS) reconstruction parameters of the PSW. The improved PSW applied correlation analysis to effectively track the degradation of bearings in variable speed. Li and Chelidze [22] successfully applied the PSW algorithm to the degradation tracking of three-dimensional (3-D) printed beam structures. The PSW algorithm effectively distinguishes damage signals from vibration signals through a hierarchical dynamical system. This framework establishes a theoretical foundation for the damage tracking based on vibration signals.

While some deep learning algorithms have achieved multivariate information fusion in machinery damage tracking, they necessitate a large amount of historical data for learning. In addition, the underlying mechanism of damage evolution is difficult to interpret [23]. Meanwhile, the physics-based PSW algorithms do not entirely utilize the multivariate signals collected by sensor networks. To overcome these deficiencies, in this article, a multivariate phase space warping (MPSW) algorithm is proposed to fully track the degradation information from multivariate signals. In the proposed MPSW, the damage evolution dynamics are considered, while the degradation patterns are simultaneously tracked in the fusion of the DIs extracted from multivariate signals. The contributions of this article are as follows.

1) The proposed MPSW algorithm provides a more suitable description of the phase space trajectory (PST) in damage tensor. The local quadratic polynomial algorithm is applied in the prediction of reference PST for multivariate signals, thereby enhancing the accuracy in tracking degradation.
2) The proposed MPSW algorithm extracts the common degradation patterns from multivariate signals. Tensor smooth constrain (TSC) algorithm is proposed in the time dimension while performing low-rank approximation. Thus, redundant information in the tensor is eliminated.
3) The proposed MPSW algorithm extracts DIs synchronously, significantly improving the accuracy of the RUL prediction. The multi-sensor information is integrated into the common degradation patterns to help enhance the RUL prediction accuracy.

The rest of this article is organized as follows. The original PSW algorithm is described in Section II. Section III introduces the principles of the proposed MPSW algorithm for tracking main degradation patterns. In Section IV, the RUL prediction approach based on the exponential degradation model is described. To validate the effectiveness of the MPSW algorithm, run-to-failure experimental datasets of bearings are utilized in Section V. Finally, Section VI concludes this article.

II. Phase Space Warping Algorithm

Vibration in rolling bearings is typically characterized by the response of dynamic models. When damage occurs in such machinery, it alters the parameters of these dynamic models, resulting in different responses and distinct vibration signals [24], [25]. Therefore, it becomes feasible to monitor the evolution of damage from vibration signals. Compared with the vibration, changes of dynamic model parameters caused by damage are assumed to be slow. To separate the slowly changing damage from rapidly changing vibration, Chelidze et al. [26] proposed the PSW algorithm, which separated fast and slow variables in the state space. The state space of the hierarchical model in PSW is expressed as follows:

$$\begin{aligned} \dot{x} &= f\left(x, \mu\left(\phi\right), t\right) \\ \dot{\phi} &= \varepsilon g\left(x, \phi, t\right) \\ s &= h\left(x\right) \end{aligned} \tag{1}$$

where $x \in \mathbb{R}^n$ represents the fast variables in the dynamical system, $\phi \in \mathbb{R}^m$ denotes the slowly changing damage process,

$\mu(\phi)$ denotes the parameter effected by ϕ, a small time scale coefficient ε is designed to connect the fast and slow variables, t denotes the time, $s \in \mathbb{R}^n$ denotes the discrete acceleration signals collected by sensors, $g(\cdot)$ is a slowly varying function, $h(\cdot)$ is measure function that links discrete signals and fast variables.

Assuming that starting from the initial moment t_0, after a short time interval t_p, the expression of the fast variable in the damaged state is

$$x\left(t_0+t_p\right)=F\left(x_0,t_0,t_p,\mu\left(\phi_0\right)\right) \tag{2}$$

where $F(\cdot)$ is the damage evolution function, x_0 represents the fast variable at t_0. To measure the effects of health and fault states on fast variables, the reference fast variables x_R in the health state are formulated as

$$x_R\left(t_0+t_p\right)=F\left(x_0,t_0,t_p,\mu\left(\phi_R\right)\right) \tag{3}$$

where ϕ_R denotes the reference damage state. Combining (2) and (3), the damage expression is extracted as follows:

$$\begin{aligned} e &= x\left(t_0+t_p\right)-x_R\left(t_0+t_p\right) \\ &= F\left(x_0,t_0,t_p,\mu\left(\phi_0\right)\right)-F\left(x_0,t_0,t_p,\mu\left(\phi_R\right)\right) \end{aligned} \tag{4}$$

where e is the damage tracking function, which reflects the change of fast variables under the damage. Slow variable damage is represented as $\Delta\phi=\phi_0-\phi_R$. At $t=t_0$ and $\phi=\phi_R$, computing the Taylor expansion for ϕ of (2) yields

$$\begin{aligned} x\left(t_0+t_p\right) &= F\left(x_0,t_0,t_p,\mu\left(\phi_0\right)\right) \\ &= F\left(x_0,t_0,t_p,\mu\left(\phi_R\right)\right) \\ &\quad+\frac{\partial F}{\partial\mu}\frac{\partial\mu}{\partial\phi}\left(\Delta\phi\right)+o(\|\Delta\phi\|^2). \end{aligned} \tag{5}$$

Substituting (3) and (5) into (4) and it gives

$$\begin{aligned} e &= x\left(t_0+t_p\right)-x_R\left(t_0+t_p\right) \\ &\approx C\left(x_0,t_0,t_p,\phi_R\right)\phi+c\left(x_0,t_0,t_p,\phi_R\right) \end{aligned} \tag{6}$$

where $C=(\partial F/\partial\mu)(\partial\mu/\partial\phi)$, and $c=-C\phi_R$. Since the time interval t_p is short, and $\Delta\phi$ is considered to be very small, the higher-order infinitesimal term $o(\|\Delta\phi\|^2)$ is ignored in (6). The damage trend is estimated by the reference damage in (6).

III. Multivariate Phase Space Warping Algorithm

A. Multivariate Phase Space Reconstruction and Reference Phase Space Trajectory Prediction

The vibration caused by damage always travels a complex transmission path before it can be received by sensors. As a result of incorrect placement of sensors, fault signatures are obscured in the acquired signal. Therefore, distributed sensor networks are applied in engineering to gather more comprehensive information. The multivariate signals are collected to extract complementary and sufficient information.

The multivariate signals are reconstructed into the high-dimensional PS by the time-delay algorithm [27], and the damage tracking function is solved in the PS to track degradation. Takens has proved that the reconstructed PS and the state space of the original system are topologically equivalent, indicating qualitative similarity in dynamical properties [28], [29]. In this article, the time delay algorithm is applied to embed the vibration signals collected by m sensors into the reconstructed PS, respectively. The expression of the d dimensional state point generated by the signal $\{s_m^i\}_{i=1}^{rl}$ collected by the mth sensor is as follows:

$$y_m^i=\left[s_m^i,s_m^{i+\tau},\ldots,s_m^{i+(d-1)\tau}\right]^T \tag{7}$$

where the embedding dimension, denoted as d, is determined using the false nearest neighbor algorithm [30], while the time delay is computed through the average mutual information algorithm [31], $y_m^i\in\mathbb{R}^{d\times1}$, and rl denoted the data length of the signals. For multivariate signals, the reconstructed PS is expressed as

$$\mathrm{Y}_m=\left[y_m^1,y_m^2,\ldots,y_m^{rl-(d-1)\tau}\right] \tag{8}$$

where $\mathrm{Y}_m\in\mathbb{R}^{d\times(rl-d\tau+\tau)}$. The PS tensor of the multi-channel signal can be obtained by constructing a 3-D matrix

$$\mathcal{Y}=[Y_1,Y_2,\ldots,Y_m] \tag{9}$$

where $\mathcal{Y}\in\mathbb{R}^{d\times(rl-d\tau+\tau)\times m}$.

Failures of mechanical equipment change the parameters of the dynamic model, and the PST of the response is also warped [32]. Due to the limited sampling frequency, the PST only qualitatively reflects the original dynamic systems, which leads to inaccuracy in linear PST prediction. To obtain an accurate description of the reference PST in the current state, a local quadratic polynomial model is constructed. The mapping P is constructed to describe the trajectories of the reconstructed PS, which is expressed as follows:

$$y_m^{i+k}=P^k\left(y_m^i,\phi\right) \tag{10}$$

where y_m^i denotes the high-dimensional PS point, y_m^{i+k} denotes the PS point after k iterations. The PST between two points satisfies multiple iterations of the mapping P and is affected by the damage ϕ. The reference PS point $y_m^R(i)$ is estimated by the current PS point y_m^i through the polynomial model

$$\begin{aligned} y_m^R(i) &= A_i\left(y_m^i\right)^2+B_iy_m^i+C_i \\ &= \theta_m(i)\,\hat{y}_m\left(i\right) \end{aligned} \tag{11}$$

where $\hat{y}_m^i$ is composed of high-dimensional PS points of each order, $\hat{y}_m(i)=[(y_m^i)^2;y_m^i;1]$, and $\theta(i)=[A_i,B_i,C_i]$.

In the PS, r local neighboring points $y_m^l(r)$ of the current damage PS are used to estimate the parameters of the polynomial model. The least squares algorithm [33] is applied to minimize the weighted loss function $J_l(\theta)$

$$J_l(\theta)=\sum_{r\in N}w_m^l(r)\left|y_m^{l+k}-\theta_m(l)\hat{y}_m^l(r)\right|^2 \tag{12}$$

where $w_m^l(r)$ denotes the weight assigned to the neighborhood points of the target, a value determined through the computation with the Epanechnikov kernel function [34]

$$w_m^l(r)=D\left(\frac{\|y_m(l)-y(l)\|}{\sigma}\right) \tag{13}$$

$$D(t) = \begin{cases} \frac{3}{4}(1-t^2), & |t| < 1 \\ 0, & \text{otherwise} \end{cases} \tag{14}$$

where σ is the neighborhood range controlled by the standard deviation. Minimize the weighted loss function $J_l(\theta)$ and it yields

$$\theta_m(l) = Y_{l+k}\left(W\hat{Y}_l\right)^T\left(\hat{Y}_l\left(W\hat{Y}\right)^T\right)^{-1} \tag{15}$$

where

$$\begin{aligned} \hat{Y}_l &= \left[\hat{y}_m^l(1), \hat{y}_m^l(2), \ldots, \hat{y}_m^l(r)\right] \\ Y_{l+k} &= \left[y_m^{l+k}(1), y_m^{l+k}(2), \ldots, y_m^{l+k}(r)\right]. \end{aligned} \tag{16}$$

Afterwards, the damage tracking function in (6) can be rewritten as

$$\begin{aligned} e_m &= \left|y_m^{i+k} - y_m^R(i)\right| \\ &\approx \left|y_m^{i+k} - \theta_m(i)\,\hat{y}_m(i)\right|. \end{aligned} \tag{17}$$

B. Tensor Smooth Constrain in the MPSW Algorithm

The damage tensor is derived from the reconstructed multivariate PS obtained from m sensors using (17). Given the high dimensionality of the multivariate PS, the accuracy of (17) is enhanced by employing the *kd*-trees algorithm to partition the space into multiple subspaces. Equation (17) is applied to extract damage within these subspaces individually and yields a more precise damage tensor. Tensor $\mathcal{Y}$ is divided into nb subspaces to extract the damage information more accurately from multivariate signals. In each subspace, the vector average algorithm is applied to extract the damage, and the average damage of the subspace is expressed as follows:

$$g_i^m(\phi) = \frac{1}{nb}\sum_{y_i \in B} e_m(y_i) \tag{18}$$

where m denotes the number of channels, i represents the number of the high-dimensional phase point, and B is the domain of the subspace. $g_i^m(\phi)$ is the average damage, ϕ represents the current damage, $e_m(\cdot)$ is the damage tracking function in (17). The damage extracted in all subspaces is composed into the damage vector, the expression is as follows:

$$G_j^m = [g_1^m(\phi), g_2^m(\phi), \ldots, g_{nb}^m(\phi)]^T \tag{19}$$

where $G_j^m \in \mathbb{R}^{nb\times 1}$, and ϕ represents the current damage. The multivariate signals are collected in real-time, and the damage vectors are extracted at the same time to assess the degradation of the machinery. The damage vectors are composed into the damage matrix, which is expressed as follows:

$$\mathrm{H}_m = [G_1^m, G_2^m, \ldots, G_{nr}^m] \tag{20}$$

where $\mathrm{H}_m \in \mathbb{R}^{nb\times nr}$. The damage matrix is constructed as the damage tensor as follows:

$$\mathcal{H} = [\mathrm{H}_1, \mathrm{H}_2, \ldots, \mathrm{H}_m] \tag{21}$$

where $\mathcal{H} \in \mathbb{R}^{nb\times nr\times m}$ is a third-order tensor. This article maintains a consistent tensor notation throughout. The third-order tensor in (21) is denoted in Euler letter font, $\mathcal{H} \in \mathbb{R}^{nb\times nr\times m}$. The format of the column fiber in tensor is $\mathcal{H}(:,j,k)$, the row fiber is $\mathcal{H}(i,:,k)$, and the tube fiber is $\mathcal{H}(i,j,:)$. Similarly, the horizontal slice is $\mathcal{H}(i,:,:)$, the lateral slice is $\mathcal{H}(:,j,:)$, and the frontal slice is $\mathcal{H}(:,:,k)$. Column fibers in damage tensor composed of damage vectors $\mathcal{H}(:,m,nr) = G_j^m$. The damage matrix of the same channel forms the lateral slice of the tensor $\mathcal{H}(:,m,:) = \mathrm{H}_m$.

The damage tensor not only contains information about the damage evolution, but also contains multi-subspace damage. While this information is complementary, it also results in redundancy. To extract common degradation from the damage tensor, we propose a tensor-robust principal component analysis algorithm that incorporates smoothness constraints.

The tube fiber $\mathcal{H}(nb,m,:) \in \mathbb{R}^{1\times nr}$ in damage tensor denotes the damage tracked in the nbth subspace of the mth channel. To isolate the smooth damage trend, this article projects the damage tensor along the time dimension to maximize the variance of the lateral slice $\mathcal{H}(:,m,:)$ while concurrently minimizing local variance

$$\max_q \|\mathcal{H}(:,m,:)\,q\|^2 \quad \text{subject to} \quad \min_q \|\mathrm{D}\mathcal{H}(:,m,:)\,q\|^2 \tag{22}$$

where $\mathrm{D}\mathcal{H}(:,m,:)$ is the difference matrix of $\mathcal{H}(:,m,:)$, q is the basis vector for smooth projection. Equation (22) can be simplified to

$$\min_q \left\{\lambda(q) = \frac{\|\mathrm{D}\mathcal{H}(:,m,:)\,q\|^2}{\|\mathcal{H}(:,m,:)\,q\|^2}\right\}. \tag{23}$$

Equation (23) is then transformed into the problem of solving eigenvalue decomposition

$$C_{DH}P = C_H P\Lambda \tag{24}$$

where C_H and C_{DH} represent the covariance matrices of $\mathcal{H}(:,m,:)$ and $\mathrm{D}\mathcal{H}(:,m,:)$ respectively. Λ is the basis vector for smooth constraints. We proposed the TSC algorithm to achieve smoothness constraints on the damage tensor. We define the tensor decomposition related functions that will be used later. The frontal slice $\mathcal{H}(:,:,k)$ of the damage tensor $\mathcal{H} \in \mathbb{R}^{nb\times nr\times m}$ are used to define the unfold$(\cdot)$ [35], [36]

$$\text{unfold}(\mathcal{H}) = [\mathrm{H}_1; \mathrm{H}_2; \ldots; \mathrm{H}_m]. \tag{25}$$

It should be noted that (25) is the transposed form of (21) under smooth constraints. The same characters are used here because they have similar meanings. Then the bcirc$(\cdot)$ is defined to implement the calculation of the block circulatory matrix

$$\text{bcirc}(H) = \begin{bmatrix} \mathrm{H}_1 & \mathrm{H}_m & \cdots & \mathrm{H}_2 \\ \mathrm{H}_2 & \mathrm{H}_1 & \cdots & \mathrm{H}_3 \\ \vdots & \vdots & \ddots & \vdots \\ \mathrm{H}_m & \mathrm{H}_{m-1} & \cdots & \mathrm{H}_1 \end{bmatrix}. \tag{26}$$

The inverse operation of the unfold function and bcirc function is defined as follows:

$$\text{fold}(\text{unfold}(\mathcal{H})) = \mathcal{H} \tag{27}$$

$$\text{bcirc}^{-1}(\text{bricr}(\mathcal{H})) = \mathcal{H}. \tag{28}$$

Since the information in the damage tensor comes from different sensors and different subspaces, the fusion of information relies on (26). The discrete Fourier transform (DFT) can realize the diagonalization of (26)

$$(\mathrm{F}_m \otimes \mathrm{I}_{nb}) \cdot \mathrm{bcirc}(\mathcal{H}) \cdot (\mathrm{F}_m^* \otimes \mathrm{I}_{nr}) = \bar{\mathrm{H}} \tag{29}$$

where $\otimes$ represents the Kronecker product, $\cdot$ denotes the standard matrix product, $\mathrm{F}_m \in \mathbb{C}^{m\times m}$ is the DFT matrix, F_m^* is the conjugate transpose of F_m, $\mathrm{F}_m\mathrm{F}_m^* = \mathrm{F}_m^*\mathrm{F}_m = m\mathrm{I}_m$, $\bar{\mathrm{H}} = \mathrm{diag}(\mathrm{D}_1, \ldots, \mathrm{D}_m)$. Miao et al. [37] have proved that the matrix D_m in (29) are diagonal if and only if the matrix H_m are diagonal

$$\mathrm{H}_i = \sum_{j=1}^{m} \omega^{(j-1)(i-1)} \mathrm{D}_i,\ i = 1, \ldots, m \tag{30}$$

where $\omega = e^{-2\pi \mathrm{i}/m}$ is a primitive mth root of unity. Then the definition of tensor product (T-product) is given [35], [36]

$$\mathcal{A} * \mathcal{B} = \mathrm{fold}(\mathrm{bcirc}(\mathcal{A}) \cdot \mathrm{unfold}(\mathcal{B})). \tag{31}$$

At the same time, the inverse operation of tensor is also defined [38], $\mathcal{A} * \mathcal{B} = \mathcal{I}$ and $\mathcal{B} * \mathcal{A} = \mathcal{I}$.

The TSC algorithm extends generalized singular value decomposition (SVD) to 3-D tensors to achieve smooth constraints on the tensors. $\mathcal{H} \in \mathbb{R}^{nb\times nr\times m}$ and $\mathrm{D}\mathcal{H} \in \mathbb{R}^{nb\times nr\times m}$ can be factored as

$$\begin{aligned} \mathcal{H} &= \mathcal{U} * \mathcal{C} * \mathcal{P} \\ \mathrm{D}\mathcal{H} &= \mathcal{V} * \mathcal{S} * \mathcal{P} \end{aligned} \tag{32}$$

where $\mathcal{U} \in \mathbb{C}^{nb\times nb\times m}$ and $\mathcal{V} \in \mathbb{C}^{nb\times nb\times m}$ are unitary, $\mathcal{C} \in \mathbb{C}^{nb\times nr\times m}$ is a f-diagonal tensor, and $\mathcal{S} \in \mathbb{C}^{nb\times nb\times m}$ is a tensor whose frontal slices $S(:,:,k)$ are lower-triangular matrices.

Therefore, the smoothness constraint problem of the damage tensor in (24) is transformed into the tensor quotient SVD. $\mathcal{P}$ represents the tensor of smooth pattern, $\mathcal{Q} = \mathcal{H} * \mathcal{P}^{-1}$ denotes the damage tensor with smoothness constraints.

C. Low-Rank Approximation in the MPSW Algorithm

The tube fibers of the smoothed damage tensor originate from various distributed sensors, resulting in different tube fibers sharing identical damage information. In other words, the forward slice of the damage tensor exhibits low rank. However, owing to variations in sensor distribution, the collected vibration signals contain interference information, which is considered sparse within the damage tensor. Consequently, we perform a low-rank approximation on the smooth-constrained damage tensor to conform the minimum tube fiber rank and eliminate redundant interference components.

The tensor robust principal component analysis (TRPCA) algorithm is applied to implement low-rank approximation of the damage tensor [39]. Damage tensor $\mathcal{H}$ can be robustly separated into a sparse tensor $\mathcal{W} \in \mathbb{R}^{nb\times m\times nr}$, and the low Tubal rank tensor $\mathcal{X} \in \mathbb{R}^{nb\times m\times nr}$, which represents the degradation. The extraction process is transformed into solving the following minimization optimization problem [39]

$$\arg\min_{\mathcal{X},\mathcal{W}} : \|\mathcal{X}\|_{TNN} + p\|\mathcal{W}\|_1, \text{s.t. } \mathcal{H} = \mathcal{X} + \mathcal{W} \tag{33}$$

where $\|\cdot\|_{TNN}$ denotes the tensor nuclear norm, p is the regularization parameter, and $\lambda = 1/\sqrt{\max(n_1 n_2) n_3}$ guarantees the optimal recovery of the tensor $\mathcal{H}$.

The damage tensor is smoothly constrained along the time dimension. The frontal slices of the damage tensor are circularly convolved to fuse the multichannel degradation information [15]. The MPSW algorithm extracts the main degradation pattern, thereby allowing the simultaneous extraction of the degradation.

IV. Remaining Useful Life Prediction Based on the Multivariate Phase Space Warping

A. Construction of Exponential Degradation Model

Upon obtaining the real-time health status of the bearing, the exponential degradation model is subsequently employed to estimate the RUL [40]. The exponential degradation models have been successfully applied by researchers to predict the RUL of batteries, bearings, and gearboxes [41], [42], [43]. To verify the tracking effect of the proposed MPSW algorithm in experiments, the exponential degradation model suitable for rolling bearings is adopted. By simulating the degradation of mechanical equipment as a random process, the constructed exponential model is expressed as follows [40]:

$$h(t) = \alpha + \theta e^{\beta t + \varepsilon - \frac{\sigma^2}{2}} \tag{34}$$

where $h(t)$ denotes the damage state at time t, α is a constant, σ and β represents two random variables that characterize the random part of the model, σ denotes the deterministic part of the stochastic process, and ε represents the random error. The estimates of stochastic parameters in exponential models are updated via Bayesian methods [40].

B. Framework of the Multivariate Phase Space Warping

The MPSW approach consists of three steps, damage extraction, degradation tracking, and RUL prediction. To better demonstrate the proposed MPSW algorithm, the flowchart of the proposed MPSW algorithm is presented in Fig. 1.

The first step of the proposed MPSW algorithm is to extract the damage from multivariate signals. The multivariate signal s_m^i is individually embedded into the reconstructed PS by the time delay algorithm. Subsequently, the MPSW employs a local quadratic polynomial model to enhance the accuracy of predicting the PST. In late-stage degradation, the original PSW algorithm must readjust reconstruction parameters to prevent significant changes in the PST and potential algorithmic failure [44]. Within a specified number of subspaces *nb*, the MPSW then identifies the warpage. These warpage values are consolidated into a damage matrix.

The second step is degradation tracking. The damage matrix evolves over time, giving rise to the development of the damage tensor. The MPSW algorithm imposes smoothness constraints

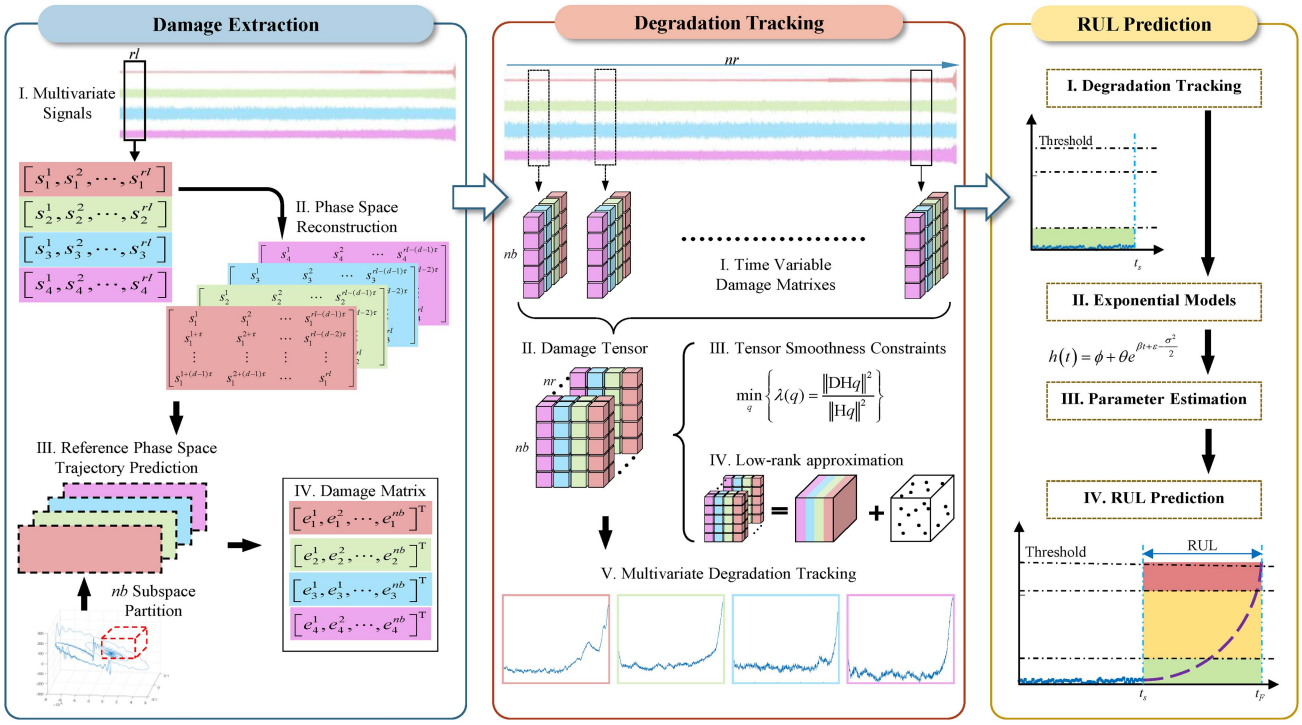

Fig. 1. Flowchart of the proposed multivariate phase space warping.

on the damage tensor along the time dimension, thereby enhancing the ability to discern degradation. Simultaneously, the MPSW algorithm executes low-rank tensor approximations and selectively extracts low-rank tube fibers to fuse the information from multiple subspaces and channels.

In the third step, the historical damage curve is utilized to fit the exponential degradation model. The model is then applied to predict the future development of real-time damage and estimate the RUL.

V. Experimental Demonstration

The bearing run-to-failure data from the intelligent maintenance systems of NSF I/UCR Center is applied to demonstrate the effectiveness of the proposed MPSW [45], and the structure of the platform is shown in the Fig. 2.

Four Rexnord ZA-2115 double-row bearings are installed on the platform, with a shaft speed of 2000 r/min and a bearing load of 6000 lbs. Four acceleration sensors are positioned to capture vibration signals, utilizing a sampling frequency of 20 kHz, a 1-s sampling time, and a 10-min sampling interval. The MPSW processes the vibration signals in real-time to assess equipment degradation and predict RUL.

The dataset comprises three sets. In set no.1, 8 sensors were employed, gathering signals over 21 560 min. Bearing three exhibited inner race defect, while bearing four displayed rolling element defects. The locations of the eight sensors are numbered in Fig. 2(b). In set no.2, four sensors were utilized, detecting an outer race failure in bearing 1 after 9840 min. The arrangement of the four sensors is marked at places numbered 1, 3, 5, and 7 in

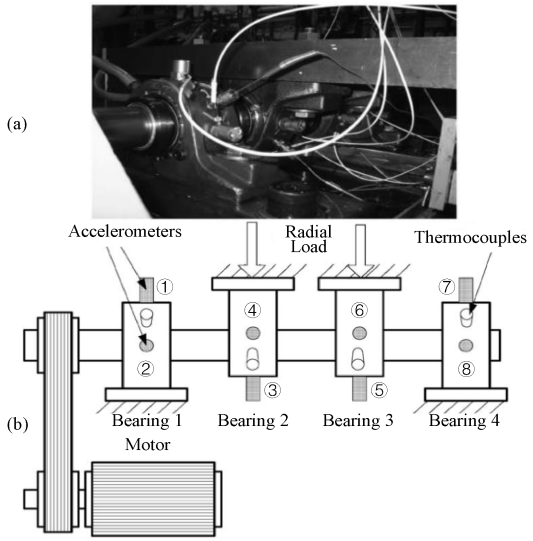

Fig. 2. Test platform of the NSF I/UCR. (a) Photograph. (b) Schematic.

Fig. 2. The no. 3 dataset involvefour sensors recording signals for 44 480 min, revealing outer race failure in bearing 3. In this article, the no. 2 dataset is utilized to showcase the benefits of the proposed MPSW algorithm for damage tracking in multisensor monitoring scenarios. The no. 1 dataset, featuring eight channels and various fault conditions, presents additional challenges for the MPSW. The no. 3 dataset is disregarded due to its matching sensor count with the no. 2.

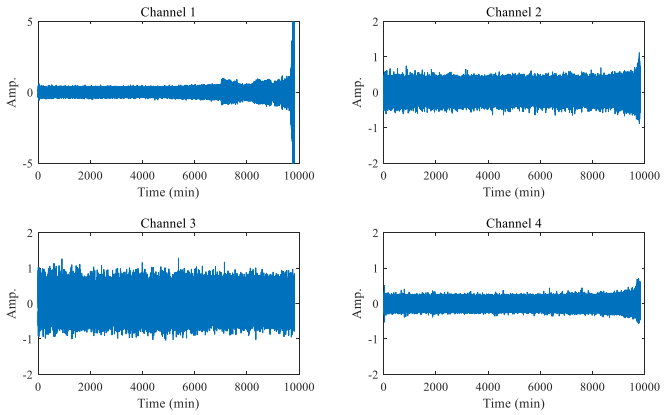

Fig. 3. Time waveforms of the signals in dataset no. 2.

TABLE I
PARAMETERS OF THE MPSW IN DATASET NO.2

m	d	nm	nb	nn	rl	λ
5	7	2^{16}	28	2^5	20 480	0.006

A. Damage Tracking for the Set No. 2

The time-domain waveforms of the vibration signals collected by the four distributed sensors are plotted in Fig. 3. It can be seen from Fig. 3 that four signals are different from each other due to different transmission paths. Additionally, there is redundancy among the signals from different sensors.

The reconstruction parameters are computed by the false nearest neighbor algorithm [30] and the mutual information algorithm [31]. The parameters are given in Table I.

In Table I, m is the time delay coefficient of the reconstructed PS, which is computed by the mutual information algorithm. d represents the embedding dimension coefficient of the reconstructed PS, which is computed by the false nearest neighbor algorithm. nm represents the number of points used for reference PS construction. nb is the number of subspaces divided in the reconstructed PS. nn is the number of nearest neighbors. rl is the number of data points monitored in real time. λ is the low-rank approximation parameters of the damage tensor. The PS is divided into 28 subspaces. Notably, the MPSW algorithm autonomously determines the nb while constructing the kd tree. Li and Chelidze [22] gave the empirical selection range of these parameters.

The time-varying warpage in the subspaces is then computed to track the damage evolution. It is difficult to display all subspaces, thus the first eight subspaces are plotted in Fig. 4 for a clearer observation. The damage extracted from different subspaces of the same channel is similar, and the damage of the equipment gradually increases with time. While the different sensor locations lead to increased disturbance of the information extracted from channels 3 and 4, which are far from the faulty bearing. Interference still exists in the degradation curve in the same subspace, posing challenges in accurately predicting the RUL.

The performance of the MPSW algorithm is compared to that of the PSW algorithm, the SVD algorithm and the TRPCA algorithm. To ensure fairness in the experiment, both the PSW and MPSW algorithm utilized same reconstruction parameters. Similarly, the TRPCA and MPSW algorithm employed (33) for parameter calculation. In the case of the SVD, the first-order singular value is chosen for reconstructing degradation curve. Figs. 5–8 show the damage extraction results for each of these three algorithms.

Damage tensors extracted from multivariate signals contain redundant information. The SVD and TRPCA are applied to decrease redundant information in the signals. However, both the PSW and SVD algorithms fail to extract complementary information in the multichannel damage matrix. The MPSW extracts complementary and common components while reducing redundancy.

Fig. 5 illustrates the effectiveness of the SVD algorithm in degradation tracking. The SVD effectively tracks damage evolution in channels 1 and 2. However, the results for channels 3 and 4 performed poorly.

Fig. 6 illustrates the tracking results of the PSW. The PSW yields a clearer multi-channel degradation curve than the SVD. Nonetheless, it still lacks the capability to determine damage at later stages.

Comparatively, Fig. 7 displays the results of each channel from the TRPCA, but the fluctuation is still large. In addition, the TRPCA exhibits an erroneous trend attributed to interference in multivariate signals of the later damage stages.

Fig. 8 presents the degradation tracking results of the MPSW algorithm, featuring a smoother degradation curve. Moreover, the degradation curve exhibits a remarkable degree of consistency, implying that the information gathered through the MPSW contains common degradation patterns of multivariate signals while eliminating interference. For a more effective comparison of tracking results across various algorithms, the degradation curves are normalized and illustrated in Fig. 9.

In Fig. 9, the multivariate damage trends extracted by the SVD fluctuate greatly with noise, making it difficult to show the degradation. Furthermore, the tracking results extracted from the signals of each channel are quite different. The SVD algorithm does not extract common patterns, which makes it difficult to evaluate the RUL. Although the PSW and TRPCA algorithm has better multichannel degradation tracking performance than the SVD, the extracted degradation patterns are inadequate. In contrast, the proposed MPSW algorithm generates a smoother degradation curve, which indicates its better ability to extract common and primary degradation pattern from multivariate signals.

Monotonicity is used as quantitative evaluation criterion for comparing degradation tracking algorithms. Based on the assumption that the damage process is irreversible, the monotonicity of the extracted degradation curve indicates that the degradation trend more closely matches the real damage trend [44], [46]. This evaluation method can determine the degradation tracking effect without knowing the real damage [47], and is commonly used in practical applications. The formula of the

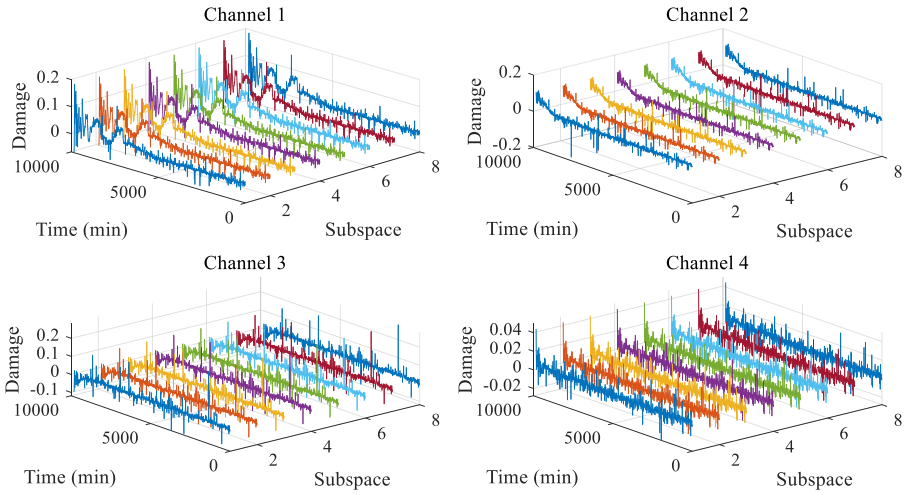

Fig. 4. Damage evolution in the first 8 subspaces out of 28.

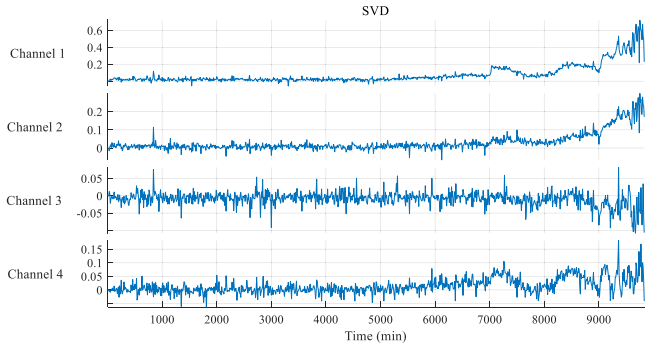

Fig. 5. Multichannel damage curves of the SVD algorithm.

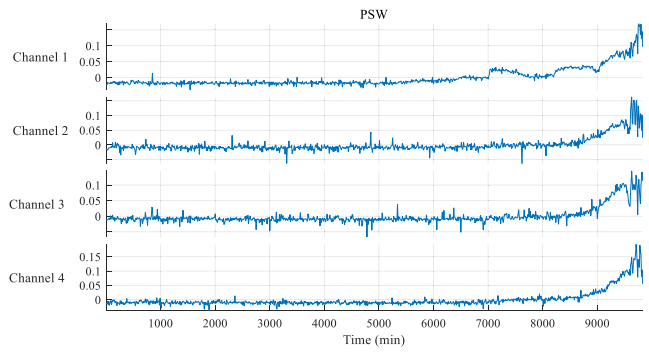

Fig. 6. Multichannel damage curves of the PSW algorithm.

monotonicity criterion is expressed as follows:

$$M = \frac{1}{n-1}\sum_{i=1}^{n-1}[\mathrm{sgn}(Y_{i+1} - Y_i)] \tag{35}$$

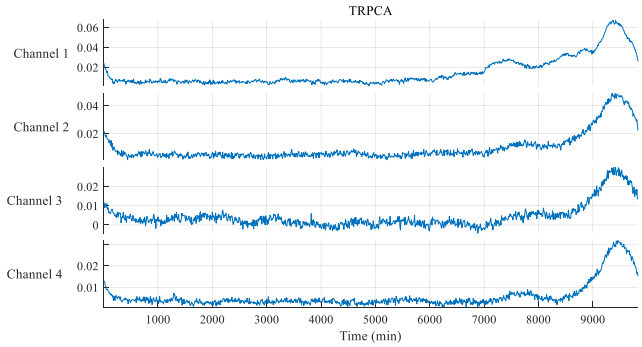

Fig. 7. Multichannel damage curves of the TRPCA algorithm.

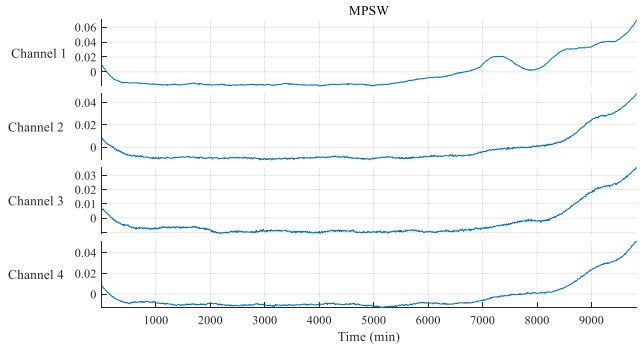

Fig. 8. Multi-channel damage curves of the MPSW algorithm.

where Y_i represents the damage, n denotes the number of the damage and $\mathrm{sgn}(\cdot)$ is the symbolic function, the expression is

$$\mathrm{sgn}(x) = \begin{cases} 1 & x > 0 \\ 0 & x = 0 \\ -1 & x < 0 \end{cases}. \tag{36}$$

Fig. 10 plots the monotonicity of degradation curves obtained by different algorithms.

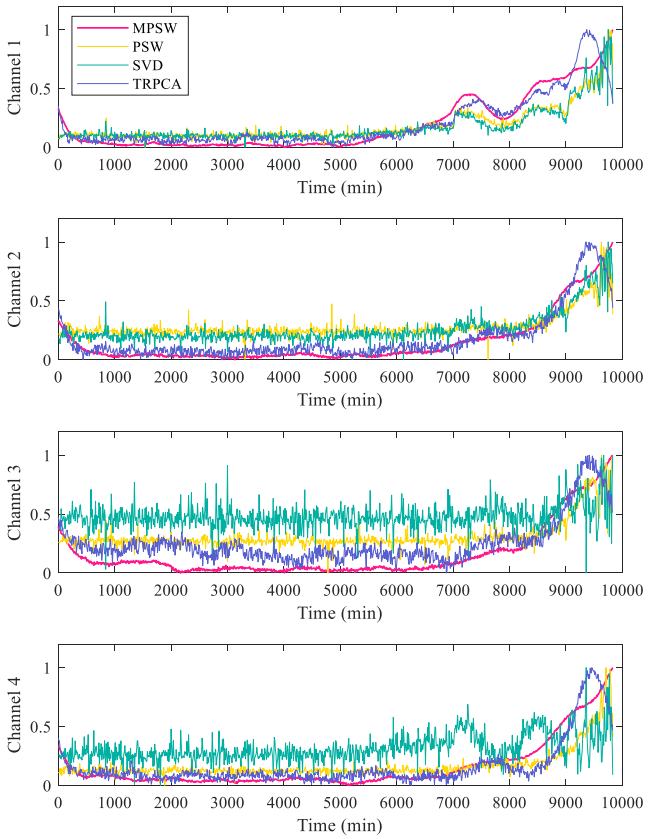

Fig. 9. Comparison of normalized damage curves of different algorithms in dataset no. 2.

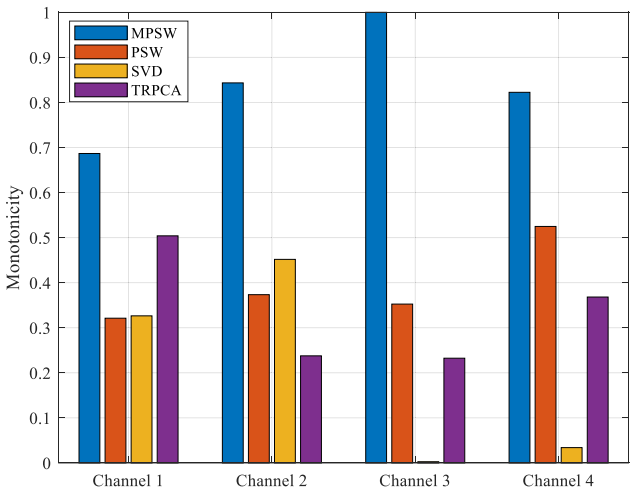

Fig. 10. Monotonicity values of the damage curves extracted by different algorithms in dataset no. 2.

The MPSW algorithm shows better degradation tracking monotonicity than the comparative algorithms in Fig. 10. Monotonicity results indicate that the MPSW algorithm has a suitable degradation trend across all channels. Compared to the PSW, TRPCA and the SVD, the proposed MPSW algorithm produces

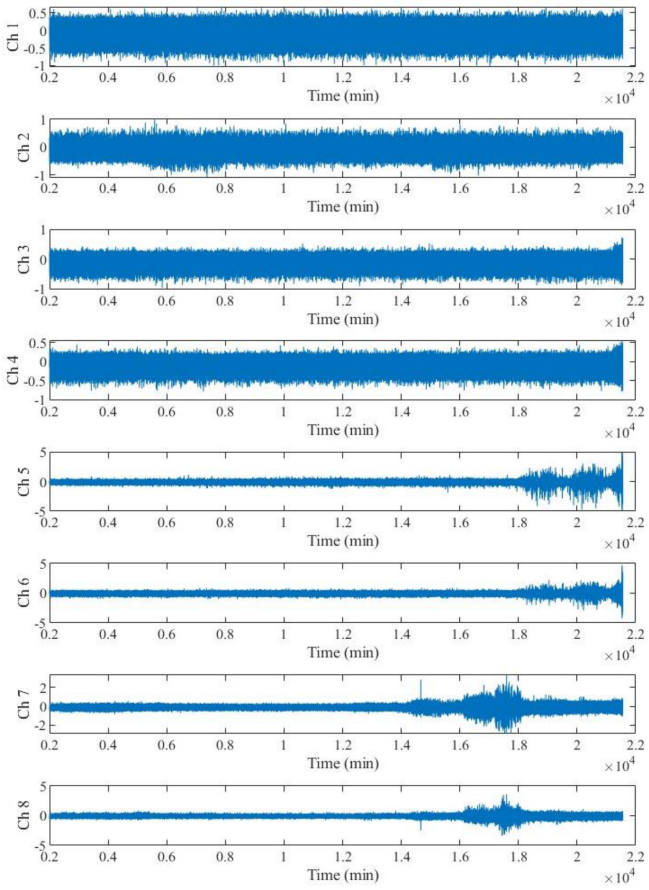

Fig. 11. Time waveforms of the signals in dataset no. 1.

TABLE II
PARAMETERS OF THE MPSW IN DATASET NO. 1

m	d	nm	nb	nn	rl	λ
5	11	2^{16}	44	2^5	20 480	0.0035

smoother degeneration tracking curves and reduces outlier interference. The outcomes demonstrate that the MPSW algorithm is more effective in tracking multivariate signal degradation.

B. Damage Tracking for the Set No. 1

To ascertain the damage tracking efficacy of the MPSW algorithm across the distributed sensors, the no. 1 dataset is employed in this section. This dataset comprises 8 channels of run-to-failure data. Following a methodology similar to that applied to dataset no. 2 in Section V-A, the MPSW algorithm proposed here conducts real-time signal processing through identical procedures. The time domain signals collected by 8 sensors are plotted in Fig. 11.

The parameters used by the proposed MPSW algorithm are given in Table II.

Fig. 12 shows the damage tracking results of different algorithms on different channels. It is evident from Fig. 12 that the proposed MPSW algorithm exhibits superior accuracy in tracking the degradation curve. Moreover, when considering

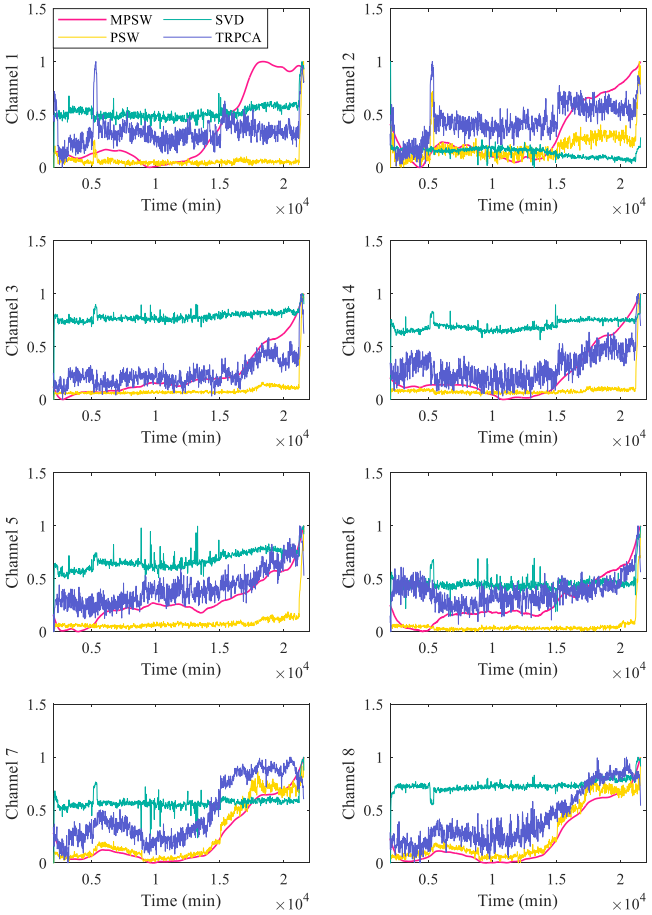

Fig. 12. Comparison of normalized damage curves of different algorithms in dataset no. 1.

distributed multisensor networks, the MPSW algorithm also shows greater advantages in all eight channels.

Analyzing the amplitude fluctuations of channels 5–8 in Fig. 11, it can be judged that bearing 3 exhibiting signs of damage at around 18 000 min, while bearing 4 showed indications of damage around 15 000 min. When integrating the information from Figs. 11 and 12, it is apparent that in scenarios involving multiple channels and multiple faults, the SVD algorithm can only effectively monitor equipment degradation in its later stages. The TRPCA algorithm tracks the main degradation patterns, but with larger fluctuations. Although the original PSW algorithm can track the degradation of bearing 4 in channels 7 and 8, the degradation of bearing 4 is not visible in the other channels. When the place of damage is unknown, the sensor arrangement might be distant from the affected component, rendering the PSW algorithm unable to monitor degradation.

However, it can be seen from Fig. 12 that the degradation curve tracked by the MPSW algorithm shows an upward trend around the 14 000th min, which can be found in the results of each channel. Furthermore, around 18 000 min, the degradation curve tracked by the MPSW algorithm also changed, signifying its capability to identify degradation in distinct device components. Notably, the MPSW algorithm effectively extracts common

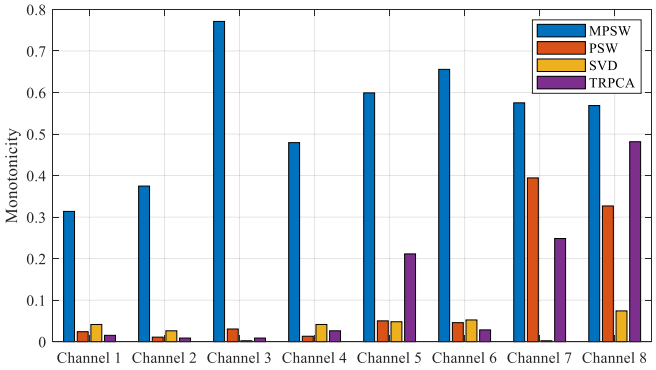

Fig. 13. Monotonicity values of the damage curves extracted by different algorithms in dataset no. 1.

degradation patterns, emphasizing critical damage information while reducing redundancy across multiple channels.

Fig. 13 shows the monotonicity values for each degradation curves. Fig. 13 illustrates the superior performance of the MPSW algorithm compared to the comparison algorithm in the monotonicity values within each channel signal. The original PSW algorithm excels only in tracking damage within channels 7 and 8, but exhibits subpar performance in other channels. The TRPCA algorithm performs better in channels 7 and 8, but is still not as good as the proposed MPSW algorithm.

C. RUL Prediction for the Set No. 2

Multivariate signals collected by the distributed sensor networks are processed by the MPSW algorithm in real time. Historical degradation data is utilized as prior information to compute parameters of the exponential model for predicting future health status and damage evolution.

This article defines the real working life as the duration of the run-to-failure experiment. Upon equipment damage, the experiment concludes, using the damage state at that moment as the threshold for predicting RUL. The stable working environment of the bearing, as evident from the experiment, indicates a lack of severe sudden collapse. Consequently, the RUL of the bearing is presumed to decrease linearly, serving as a reference for algorithm performance.

Fig. 14 displays four subgraphs, each revealing the RUL prediction outcomes of various algorithms. The abscissa axis in the subgraph represents the current working time, and the ordinate axis denotes the RUL. The scatter points represent the RUL predicted by different algorithms at the corresponding time. Based on the assumption that equipment degradation is linear, the red dotted line indicates the actual RUL.

Fig. 14(a) plots the RUL results of the degradation tracked by the SVD algorithm in the exponential degradation model. Unfortunately, this algorithm has a disparity between its predictions and reality.

In Fig. 14(b), the RUL of the PSW algorithm perform well in the later stage of the damage. However, the early DIs tracked by the PSW algorithm often produces outliers that interfered with RUL prediction results. The PSW and SVD algorithms

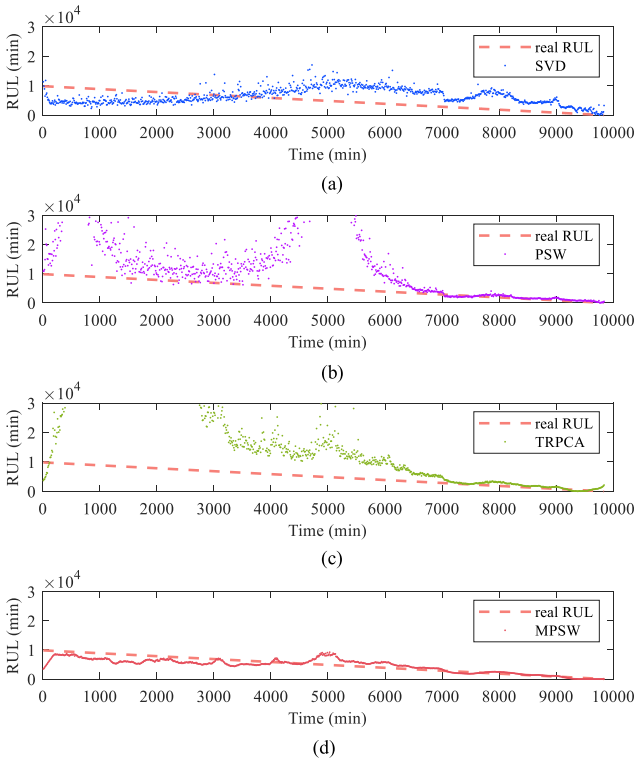

Fig. 14. RUL prediction results of the three algorithms for channel 1. (a) Singular value decomposition. (b) Phase space warping. (c) Tensor robust principal component analysis. (d) Multivariate phase space warping.

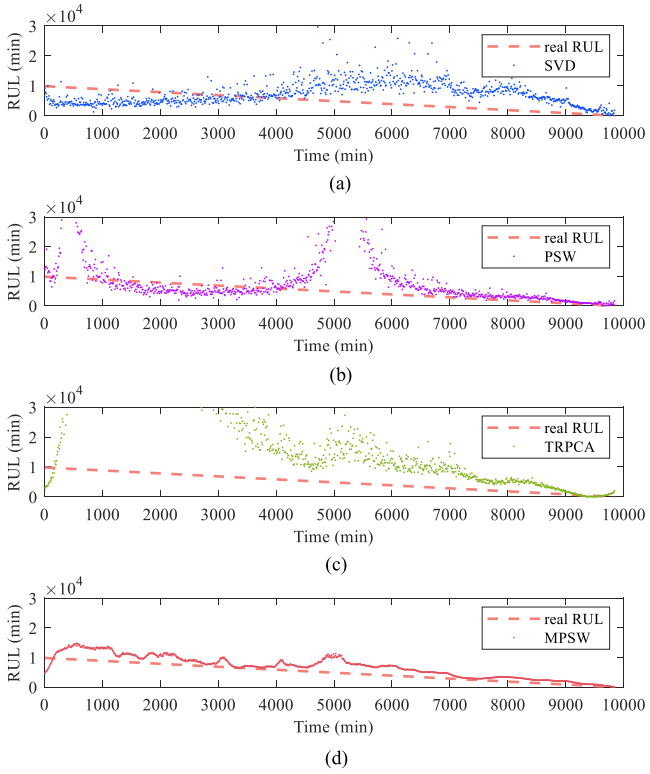

Fig. 15. RUL prediction results of the three algorithms for channel 2. (a) Singular value decomposition. (b) Phase space warping. (c) Tensor robust principal component analysis. (d) Multivariate phase space warping.

only extract the damage from single-channel signals instead of multivariate signals, therefore leading to inaccurate RUL.

Fig. 14(c) plots the RUL results of the degradation pattern of the TRPCA algorithm. It can be seen from Fig. 14 that although the RUL prediction in the later damage stage is accurate, but the deviation in the early stage is large.

In Fig. 14(d), the proposed MPSW algorithm results exhibit better linearity and improved fitting of the real RUL. Notably, the multivariate degradation extraction capacity of the MPSW algorithm enables it to detect common degradation patterns in multivariate signals, thus yielding higher accuracy in RUL prediction. The signals from the remaining three channels are tracked and predicted RUL in real time. The results are plotted in Figs. 15–17.

Among the results in Figs. 14–17, the predicted RUL based on SVD is far from the actual RUL. The reason for this discrepancy can be attributed to the fact that the SVD is unable to capture the main degradation patterns in multivariate signals.

From Figs. 14–17, it is evident that the predictions based on the PSW and TRPCA algorithms are accurate during the later stages of damage. Their results from different channels also exhibit similarities. Combining with Fig. 9, it can be inferred that the fluctuation of the curve conceals the slight damage evolution, which leads to errors in the training of the exponential degradation model.

The RUL values of the MPSW jump at the beginning, which is due to the running-in of machinery. By effectively extracting

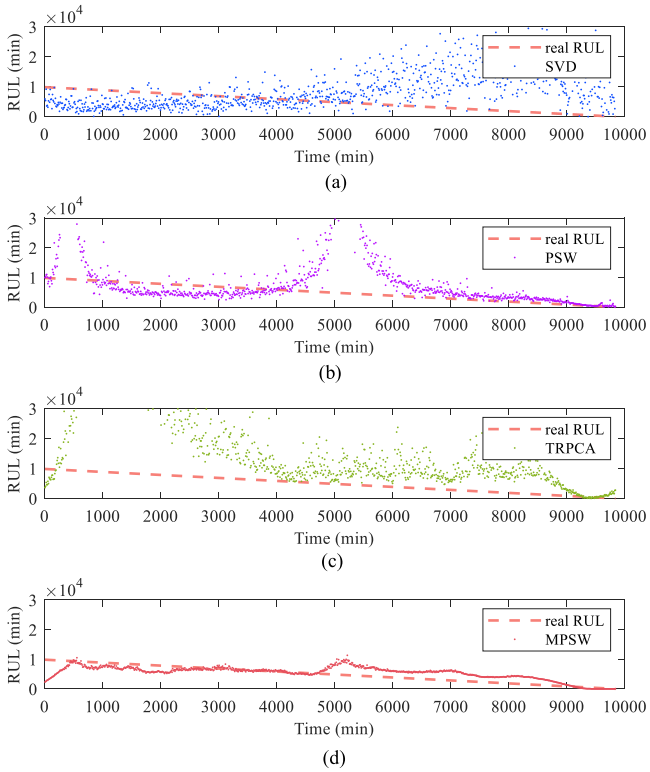

Fig. 16. RUL prediction results of the three algorithms for channel 3. (a) Singular value decomposition. (b) Phase space warping. (c) Tensor robust principal component analysis. (d) Multivariate phase space warping.

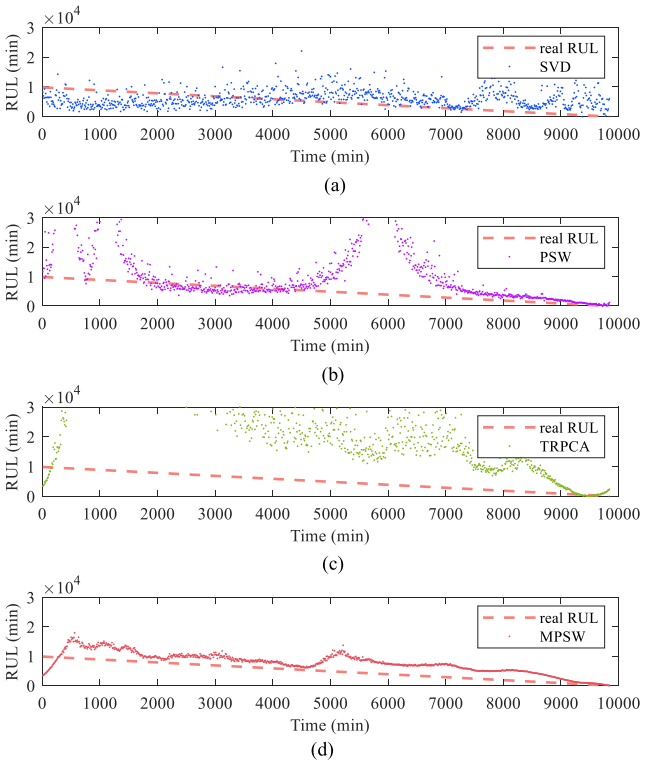

Fig. 17. RUL prediction results of the three algorithms for channel 4. (a) Singular value decomposition. (b) Phase space warping. (c) Tensor robust principal component analysis. (d) Multivariate phase space warping.

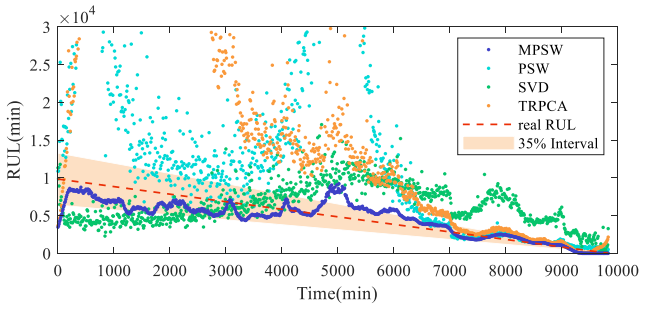

Fig. 18. RUL results of different algorithms in dataset no. 2.

common degradation patterns from multivariate signals, the degradation model based on the MPSW yields more accurate predictions of RUL. The 35% interval of the real RUL is plotted in Fig. 18 to demonstrate the prediction accuracy based on different algorithms.

To express the impact of the degradation tracked by the algorithms on the RUL prediction, the R-square (R^2) is applied to test the effect of the RUL prediction of different algorithms [48], [49]. The expression of the R^2 is as follows:

$$\mathrm{R}^2 = 1 - \frac{\sum_i \left(\hat{h}_i - h_i\right)^2}{\sum_i \left(\bar{h} - h_i\right)^2} \tag{37}$$

TABLE III
R^2 VALUES OF THE RESULTS ON RUL PREDICTION

Channels	Algorithms			
	MPSW	PSW	SVD	TRPCA
Channel 1	0.7206	0.0068	0.0087	0.3703
Channel 2	0.8560	0.0031	0.0248	0.3427
Channel 3	0.4823	0.0072	0.3027	0.4237
Channel 4	0.7192	0.0147	0.0087	0.4736

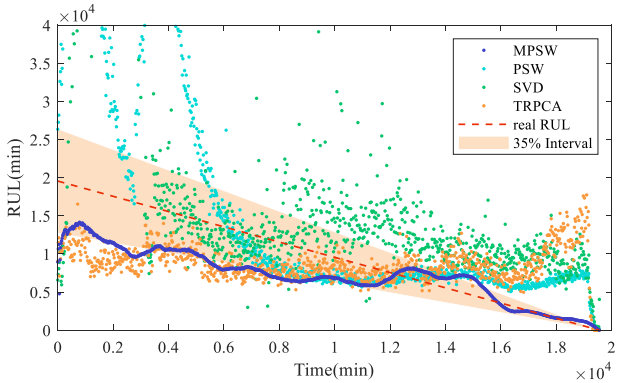

Fig. 19. RUL results of different algorithms in dataset no. 1.

where h_i denotes the true RUL value at time i, $\bar{h}$ represents the mean value of the true RUL value, and $\hat{h}_i$ represents the predicted RUL value at time i. A larger value of R^2 indicates that the predicted RUL is closer to the real RUL. The RUL prediction process of different algorithms is analyzed using the R^2 indicator, and the results are given in Table III.

In Table III, the MPSW algorithm predicts the RUL with higher accuracy than the comparative algorithms. By incorporating the characteristics of multiple signals, the MPSW algorithm fits the exponential degradation model better.

D. RUL Prediction for the Set No. 1

Same as the operation in Section V-C, the damage tracking results from the eight sensors in dataset no.1 are input into the exponential model to predict the evolution trend. The RUL prediction results of the degradation curves tracked by different algorithms are plotted in Fig. 19.

As can be seen from Fig. 19, the RUL result of the MPSW algorithm is more consistent with the linear decreasing trend. In addition, there is an increase at the beginning of the curve of the MPSW algorithm, which is considered to be caused by the equipment running-in period. For clarity of presentation, Fig. 20 is the zoom in view of part of the Fig. 19.

Fig. 20 illustrates a rapid decline in RUL at approximately the 15 000th min, aligning with the failure of bearing 3 as indicated by the time domain signal. However, the original PSW algorithm fails to effectively capture the degradation of bearing 3. Comparatively, the SVD, PSW, and TRPCA algorithms struggle to fulfill the requirements of predictive maintenance. When mechanical equipment experiences degradation of multiple fault types, the MPSW algorithm extracts the common degradation patterns in

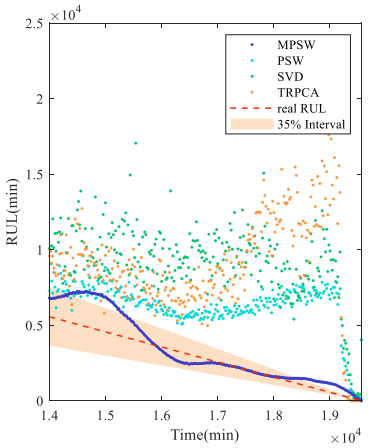

Fig. 20. Enlarged view of the RUL prediction results in dataset no. 1.

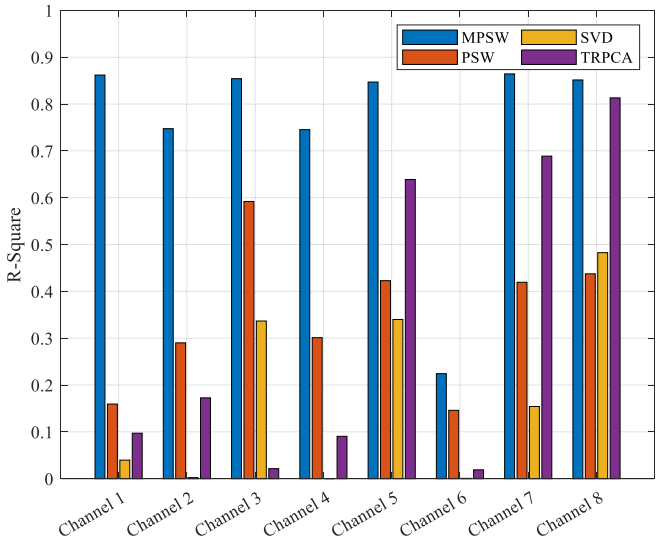

Fig. 21. R^2 values of the RUL result in dataset no. 1.

multivariate signals, thereby enhancing the reliability of RUL predictions.

Fig. 21 shows the R^2 values comparing the predicted RUL with the actual RUL, serving as an indicator of prediction accuracy. The R^2 values for each channel in the MPSW algorithm outperform those of the comparative method, underscoring the superior representation of shared damage patterns in the MPSW prediction model.

The RUL prediction accuracy results indicate that the proposed MPSW algorithm can track the damage evolution in multivariate signals simultaneously when coupled with the exponential degradation model. As a result, the MPSW algorithm is more suitable for predictive maintenance applications due to the higher-precision RUL.

VI. Conclusion

This article was primarily concerned with the problem of degradation tracking and RUL prediction of mechanical equipment monitored by distributed sensor networks, while also considering the relationship between damage dynamic behavior and damage evolution. The MPSW algorithm was proposed for monitoring the primary degradation of rolling bearings. Experimental run-to-failure tests on bearings are adopted to validate the effectiveness of the proposed MPSW.

1) The results of the MPSW algorithm exhibit reduced fluctuations compared to the original PSW results. This improvement was attributed to the enhanced prediction of the reference PST.
2) The MPSW algorithm provides the consistent information in tracking multivariate degradation. In contrast, the curves tracked by the comparison method contain more redundant information, which interferes with the prognosis.
3) The MPSW algorithm significantly enhances the accuracy of RUL prediction by effectively identifying common degradation patterns within multivariate signals. This leads to an efficient parameter estimation of RUL model.

In future work, the MPSW algorithm will be extended to RUL prediction of multivariate signals from different devices. In addition, we will further reduce the algorithm complexity while improving feature extraction capabilities.

References

[1] A. Heng, S. Zhang, A. C. C. Tan, and J. Mathew, "Rotating machinery prognostics: State of the art, challenges and opportunities," *Mech. Syst. Signal Process.*, vol. 23, no. 3, pp. 724–739, Apr. 2009.
[2] Y. Lei, N. Li, L. Guo, N. Li, T. Yan, and J. Lin, "Machinery health prognostics: A systematic review from data acquisition to RUL prediction," *Mech. Syst. Signal Process.*, vol. 104, pp. 799–834, May 2018.
[3] M. Kordestani, M. Saif, M. E. Orchard, R. Razavi-Far, and K. Khorasani, "Failure Prognosis and applications—A survey of recent literature," *IEEE Trans. Rel.*, vol. 70, no. 2, pp. 728–748, Jun. 2021.
[4] H. Song, R. Yuan, Y. Lv, H. Pan, and X. Yang, "Improved two-dimensional multiscale fractional dispersion entropy: A novel health condition indicator for fault diagnosis of rolling bearings," *IEEE Sens. J.*, vol. 24, no. 3, pp. 3431–3444, Feb. 2024.
[5] H. Luo, S. Yang, X. Hu, and X. Hu, "Agent oriented intelligent fault diagnosis system using evidence theory," *Expert Syst. Appl.*, vol. 39, no. 3, pp. 2524–2531, Feb. 2012.
[6] D. Wang and K. Tsui, "Theoretical investigation of the upper and lower bounds of a generalized dimensionless bearing health indicator," *Mech. Syst. Signal Process.*, vol. 98, pp. 890–901, Jan. 2018.
[7] P. Ding, M. Jia, Y. Ding, Y. Cao, J. Zhuang, and X. Zhao, "Machinery probabilistic few-shot prognostics considering prediction uncertainty," *IEEE/ASME Trans. Mechatron*, early access, May 12, 2023, doi: 10.1109/tmech.2023.3270901.
[8] X. Zhang, R. Xu, C. Kwan, S. Y. Liang, Q. Xie, and L. Haynes, "An integrated approach to bearing fault diagnostics and prognostics," in *Proc., Amer. Control Conf.*, 2005, vol. 4, pp. 2750–2755.
[9] X. Liu, Y. Lei, N. Li, X. Si, and X. Li, "RUL prediction of machinery using convolutional-vector fusion network through multi-feature dynamic weighting," *Mech. Syst. Signal Process.*, vol. 185, Feb. 2023, Art. no. 109788.
[10] B. Ayhan, C. Kwan, and S. Y. Liang, "Adaptive remaining useful life prediction algorithm for bearings," in *Proc. IEEE Int. Conf. Prognostics Health Manage.*, 2018, pp. 1–8.
[11] X. Zhao et al., "Model-assisted muti-source fusion Hypergraph Convolutional Neural networks for intelligent few-shot fault diagnosis to Electro-hydrostatic actuator," *Inf. Fusion*, vol. 104, Apr. 2024, Art. no. 102186.
[12] J. Xiong, D. W. Coit, Y. Ma, F. Zhang, and C. Lin, "Adaptive deep learning-based remaining useful life prediction framework for systems with multiple failure patterns," *Rel. Eng. System Saf.*, vol. 235, Jul. 2023, Art. no. 109244.
[13] N. Li, N. Gebraeel, Y. Lei, X. Fang, X. Cai, and T. Yan, "Remaining useful life prediction based on a multi-sensor data fusion model," *Rel. Eng. Syst. Saf.*, vol. 208, Apr. 2021, Art. no. 107249.

[14] Y. Lv, R. Yuan, and G. Song, "Multivariate empirical mode decomposition and its application to fault diagnosis of rolling bearing," *Mech. Syst. Signal Process.*, vol. 81, pp. 219–234, Dec. 2016.
[15] Q. Zhang, R. Yuan, Y. Lv, Z. Li, and H. Wu, "Multivariate dynamic mode decomposition and its application to bearing fault diagnosis," *IEEE Sensors J.*, vol. 23, no. 7, pp. 7514–7524, Apr. 2023.
[16] R. Yuan, Y. Lv, T. Wang, S. Li, and H. Li, "Looseness monitoring of multiple M1 bolt joints using multivariate intrinsic multiscale entropy analysis and Lorentz signal-enhanced piezoelectric active sensing," *Struct. Health Monit.*, vol. 21, no. 6, pp. 2851–2873, Mar. 2022.
[17] J. P. Cusumano and D. Chelidze, "Phase space warping: A dynamical systems approach to diagnostics and prognostics," *Solid Mechanics Appl.*, vol. 122, pp. 183–192, Dec. 2005.
[18] D. Chelidze and M. Li, "Dynamical systems approach to fatigue damage identification," *J. Sound Vib.*, vol. 281, no. 3–5, pp. 887–904, Mar. 2005.
[19] D. Chelidze and J. P. Cusumano, "Phase space warping: Nonlinear time-series analysis for slowly drifting systems," *Math Phys. Eng. Sci.*, vol. 364, no. 1846, pp. 2495–2513, Jul. 2006.
[20] Y. Qian, R. Yan, and R. X. Gao, "A multi-time scale approach to remaining useful life prediction in rolling bearing," *Mech. Syst. Signal Process.*, vol. 83, pp. 549–567, Jan. 2017.
[21] P. Luo, N. Hu, L. Zhang, J. Shen, and Z. Cheng, "Improved phase space warping method for degradation tracking of rotating machinery under variable working conditions," *Mech. Syst. Signal Process.*, vol. 157, Aug. 2021, Art. no. 107696.
[22] H. Li and D. Chelidze, "Geometry-informed phase space warping for reliable fatigue damage monitoring," *Struct. Health Monit.*, Jul. 2023, doi: 10.1177/14759217231174894.
[23] W. Wang, Y. Lei, T. Yan, N. Li, and A. Nandi, "Residual convolution long short-term memory network for machines remaining useful life prediction and uncertainty quantification," *JDMD*, vol. 1, no. 1, pp. 2–8, Dec. 2021, doi: 10.37965/jdmd.v2i2.43.
[24] L. Cui, Y. Zhang, F. Zhang, J. Zhang, and S.-C. Lee, "Vibration response mechanism of faulty outer race rolling element bearings for quantitative analysis," *J. Sound Vib.*, vol. 364, pp. 67–76, Mar. 2016.
[25] Q. Niu and S. Yang, "Study on fatigue degradation behavior of a cracked rotor subjected to lateral vibration," *Shock Vib.*, vol. 2018, 2018, Art. no. 3239523.
[26] D. Chelidze, J. P. Cusumano, and A. Chatterjee, "A dynamical systems approach to damage evolution tracking, part 1: Description and experimental application," *J. Vib. Acoust.*, vol. 124, no. 2, pp. 250–257, Mar. 2002.
[27] N. H. Packard, J. P. Crutchfield, J. D. Farmer, and R. S. Shaw, "Geometry from a time series," *Phys. Rev. Lett.*, vol. 45, no. 9, pp. 712–716, Sep. 1980.
[28] F. Takens, "Detecting strange attractors in turbulence," in *Dynamical Systems and Turbulence, Warwick 1980*, D. Rand and L. Young, eds., Berlin, Heidelberg: Springer, 1981, pp. 366–381.
[29] H. Li, E. D. Gedikli, and R. Lubbad, "Exploring timedelaybased numerical differentiation using principal component analysis," *Physica A, Stat. Mechanics Appl.*, vol. 556, Nov. 2020, Art. no. 124839.
[30] M. B. Kennel, R. Brown, and H. D. I. Abarbanel, "Determining embedding dimension for phase-space reconstruction using a geometrical construction," *Phys. Rev. A*, vol. 45, no. 6, pp. 3403–3411, Mar. 1992.
[31] A. M. Fraser and H. L. Swinney, "Independent coordinates for strange attractors from mutual information," *Phys. Rev. A*, vol. 33, no. 2, pp. 1134–1140, Feb. 1986.
[32] H. Liu, R. Yuan, Y. Lv, X. Yang, H. Li, and G. Song, "Degradation tracking of rolling bearings based on local polynomial phase space warping," *IEEE Trans. Rel.*, early access, Dec. 2023, doi: 10.1109/TR.2023.3335899.
[33] J. Gu, Q. Li, and J. Yang, "Multivariate local polynomial kernel estimators: Leading bias and asymptotic distribution," *Econometric Rev.*, vol. 34, no. 6–10, pp. 979–1010, 2015.
[34] P. A. Moraes, D. G. Fantinato, and A. Neves, "Epanechnikov kernel for PDF estimation applied to equalization and blind source separation," *Signal Process.*, vol. 189, Dec. 2021, Art. no. 108251.
[35] M. Ge, Y. Lv, and Y. Ma, "Research on multichannel signals fault diagnosis for bearing via generalized non-convex tensor robust principal component analysis and tensor singular value kurtosis," *IEEE Access*, vol. 8, pp. 178425–178449, 2020.
[36] Z. He, "Generalized singular value decompositions for tensors and their applications," *Numer. Math. Theory Methods Appl.*, vol. 14, no. 3, pp. 692–713, Jun. 2021.
[37] Y. Miao, L. Qi, and Y. Wei, "T-Jordan canonical form and T-drazin inverse based on the T-product," *Commun. Appl. Math. Comput.*, vol. 3, no. 2, pp. 201–220, 2021.
[38] M. E. Kilmer and C. D. Martin, "Factorization strategies for third-order tensors," *Linear Algebra Appl.*, vol. 435, no. 3, pp. 641–658, Aug. 2011.
[39] C. Lu, J. Feng, Y. Chen, W. Liu, Z. Lin, and S. Yan, "Tensor robust principal component analysis with a new Tensor nuclear norm," *IEEE Trans. Pattern Anal. Mach. Intell.*, vol. 42, no. 4, pp. 925–938, Apr. 2020.
[40] N. Z. Gebraeel, M. A. Lawley, R. Li, and J. K. Ryan, "Residual-life distributions from component degradation signals: A Bayesian approach," *IIE Trans.*, vol. 37, no. 6, pp. 543–557, Jun. 2005.
[41] N. Li, Y. Lei, J. Lin, and S. X. Ding, "An improved exponential model for predicting remaining useful life of rolling element bearings," *IEEE Trans. Ind. Electron.*, vol. 62, no. 12, pp. 7762–7773, Dec. 2015.
[42] G. Wang and J. Xiang, "Remain useful life prediction of rolling bearings based on exponential model optimized by gradient method," *Measurement*, vol. 176, May 2021, Art. no. 109161.
[43] W. Song, H. Liu, and E. Zio, "Long-range dependence and heavy tail characteristics for remaining useful life prediction in rolling bearing degradation," *Appl. Math. Modelling*, vol. 102, pp. 268–284, Feb. 2022.
[44] H. Liu, R. Yuan, Y. Lv, H. Li, E. D. Gedikli, and G. Song, "Remaining useful life prediction of rolling bearings based on segmented relative phase space warping and particle filter," *IEEE Trans. Instrum. Meas.*, vol. 71, Jan. 2022, Art. no. 3527415.
[45] H. Qiu, J. Lee, J. Lin, and G. Yu, "Wavelet filter-based weak signature detection method and its application on rolling element bearing prognostics," *J. Sound Vib.*, vol. 289, no. 4–5, pp. 1066–1090, Feb. 2006.
[46] J. Coble and J. W. Hines, "Identifying optimal prognostic parameters from data: A genetic algorithms approach," in *Proc. Annu. Conf. PHM Soc.*, Mar. 2021, vol. 1, no. 1. [Online]. Available: https://www.papers.phmsociety.org/index.php/phmconf/article/view/1404
[47] G. Zhang, Y. Wang, X. Li, Y. Qin, and B. Tang, "Dynamic evaluation of degradation space variation for machine condition monitoring," *IEEE Trans. Instrum. Meas.*, vol. 71, Jan. 2022, Art. no. 3517810.
[48] X. Jin, Y. Sun, Z. Que, Y. Wang, and T. W. S. Chow, "Anomaly detection and fault prognosis for bearings," *IEEE Trans. Instrum. Meas.*, vol. 65, no. 9, pp. 2046–2054, Sep. 2016.
[49] A. Gelman, B. Goodrich, J. Gabry, and A. Vehtari, "R-squared for Bayesian regression models," *Amer. Statistician*, vol. 73, no. 3, pp. 307–309, May 2019.